








## Research Article

# Nucleus Disc Replacement: Design and Material Selection FEA Analysis

**Amparo Vanaclocha** <sup>1</sup>, **Vicente Vanaclocha** <sup>2</sup>, **Carlos M. Atienza** <sup>3,4</sup>, **Pablo Clavel**<sup>5</sup>,  
**Pablo Jorda-Gomez** <sup>6</sup>, **Carlos Barrios** <sup>7</sup>, **Nieves Saiz-Sapena** <sup>8</sup>,  
**and Leyre Vanaclocha** <sup>9</sup>

<sup>1</sup>Escuela de Doctorado, Universitat Politècnica de Valencia, Camí de Vera, s/n, Valencia 46022, Spain

<sup>2</sup>University of Valencia, Valencia, Avenida de Blasco Ibáñez, 15, Valencia 46010, Spain

<sup>3</sup>Instituto de Biomecánica (IBV), Universitat Politècnica de Valencia, Camí de Vera, s/n, Valencia 46022, Spain

<sup>4</sup>Instituto de Biomecánica de Valencia-CIBER BBN, Grupo de Tecnología Sanitaria (GTS-IBV), Camí de Vera, s/n, Valencia 46022, Spain

<sup>5</sup>Instituto Clavel, Hospital Quironsalud Barcelona, Plaça d'Alfonso Comín 5, Barcelona 08023, Spain

<sup>6</sup>Hospital General Universitario de Castellón, Avenida de Benicàssim 128, Castelló de la Plana 12004, Spain

<sup>7</sup>Catholic University of Valencia, Saint Vincent Martyr, Carrer de Quevedo 2, Valencia 46001, Spain

<sup>8</sup>Hospital General Universitario de Valencia, Avenida Tres Cruces 2, Valencia, Spain

<sup>9</sup>Medius Klinik, Ostfildern-Ruit Klinik für Urologie, Hedelfinger Strasse 166, 73760 Ostfildern, Esslingen, Baden-Wurtemberg, Germany

Correspondence should be addressed to Vicente Vanaclocha; [vicente.vanaclocha@uv.es](mailto:vicente.vanaclocha@uv.es)

Received 2 August 2022; Revised 2 October 2022; Accepted 10 October 2022; Published 31 October 2022

Academic Editor: Hao Yi

Copyright © 2022 Amparo Vanaclocha et al. This is an open access article distributed under the Creative Commons Attribution License, which permits unrestricted use, distribution, and reproduction in any medium, provided the original work is properly cited.

*Study Design.* We selected the materials and implant design and performed Finite Element Analysis (FEA) studies. *Background.* Nucleus disc replacements, implanted since 1960, have undergone continuous evolution in materials and designs, but subsidence, extrusion, and *in vivo* degradation limit widespread use. *Aim.* The aim of this study is to create a new nucleus disc replacement that avoids the abovementioned drawbacks. *Material and Methods.* We created eighteen designs with varied materials and analyzed them with FEA in compression and shear tests in a lumbar spine model programmed in Ansys Parametric Design Language. *Results.* Bionate® 80A had the closest mechanical characteristics to the intact disc nucleus. Monobloc designs bore physiological stresses correctly but suffered significant deformations with permanent damage during surgical insertion through the annulus opening. In addition, sandwich designs were too rigid and had an unreliable curing process. Therefore, we chose an oval doughnut-like 5 mm wall monobloc Bionate® 80A nucleus replacement. It minimized implant stress in loading, distributed loads uniformly, and tolerated lateral compression during implantation. *Conclusions.* Out of the eighteen designs we analyzed with FEA, we found that the monobloc oval doughnut-like Bionate 80A nucleus replacement reproduced best the biomechanics of the natural disc nucleus and had the lowest subsidence risk as it transmits the load to the ring apophysis. Furthermore, implanting it through the annulotomy required to perform a lumbar microdiscectomy should be possible due to its elasticity. Furthermore, due to its elasticity implanting it through the average annulotomy required to perform a lumbar microdiscectomy should be possible.

## 1. Introduction

Chronic low back pain keeps being one of the most common human ailments [1]. One of its causes is degenerative disc disease, which can lead to disc herniation. The standard

treatment for these cases is a discectomy, frequently followed by spinal arthrodesis. In both events, the index level undergoes biomechanical changes that cause arthritic changes in this level [2] and adjacent ones [3]. Therefore, the best approach would be to replace the function of the damaged intervertebral discs.

Nucleus replacement (NR) devices aim to substitute the nucleus pulposus with an intact annulus fibrosus. This technique is less invasive than spinal fusion or total disc replacement to treat disc herniation or degenerative disc disease.

A nucleus replacement should restore vertebral alignment, physiological curvature, instantaneous center of rotation, and disc height without overstressing spinal ligaments or zygapophyseal joint capsules, allow six degrees of freedom [4] and provide a close fit to the vertebral endplates [4–6]. It must be biocompatible, stiff, possess viscoelastic behavior and shock absorption capacity similar to the intact nucleus [7], and avoid stress shielding [7, 8].

Mechanical characteristics should mimic the intact disc with nonlinear viscoelastic behavior. It should withstand 800–2500 N in axial compression [9], 700–1000 N standing up upright [10], 2400 N/mm standing up with the trunk flexed forward 30° [11], 1800–2700 N sitting [12], 4000–4200 N lifting a 200 N load while bending forward [13], and 31.5 Nm in 2.0 Nm/° axial torsion [14]. It should also have a  $5.39 \pm 2.56$  kPa linear-region modulus, 4.2 MPa Young's modulus [15], and 0.49 Poisson's ratio [16]. The swelling pressure is 0.11–0.14 MPa [16], shear modulus is 7.4–19.8 kPa [17], and vertebral endplate compression  $6.5 \pm 2.5$  kN [18].

Target mechanical properties for the whole disc after nucleus replacement (intact annulus+nucleus prosthetic device) are compressive strength >6.5 kN, shear strength >3 kN, compressive fatigue strength >2500 N, wear tests 900–1850 N–10 million cycles, shear force fatigue strength >100 N, torsion torque fatigue strength >3.5 Nm, and stiffness: 800–2500 N/mm. In addition, it must have a high wear resistance with minimal debris generation, optimal long-term performance (30–100 million cycles), and compatibility with CT and MRI.

The initial biomechanical evaluation through finite element analysis (FEA) allows cost saving, design improvement, and product optimization. In addition, it enables implant mechanical behavior reproduction and analysis of surrounding spinal structure response (annulus, ligaments, vertebral endplates, and zygapophyseal joints) [19–23]. This information is essential to validate the spinal implant, restore the lumbar spine's biomechanics, and minimize abnormal loading on surrounding anatomical structures [24].

Introduced in the 60's, there has been a steady search to find a material that reproduces intact disc biomechanics, creating a design that is easy to insert and with a minimal risk of subsidence or extrusion. Silicones, diverse polymers, hydrogels, and polyurethanes (PU) have been tested and ruled out because of cracking [25], subsidence [26], or extrusion [27]. In addition, researchers have improved designs continuously to ease insertion. Researchers have recently introduced new materials like nanofibers [28], providing a scaffold for cell ingrowth and revitalization [29]. Leading research groups have tested different materials [30], and stem cells [31], both autologous and heterologous, are being used, but none of these new strategies have yet reached clinical application.

The purpose of our study was to test different materials and create different designs to reach a specific implant complying with the requirements mentioned above.

## 2. Material and Methods

Finite element analysis (FEA) helps in implant mechanical behavior reproduction and surrounding spinal structure response evaluation (annulus, ligaments, vertebral endplates, and zygapophyseal joints). This information is crucial to validate any spinal implant before undertaking further steps. It allows cost saving, design improvement, and product optimization [21].

First, we created the finite element analysis (FEA) model using data from cadaveric human lumbosacral spines that we reported in a previous publication [32]. In short, we used twelve lumbosacral spine specimens from fresh, cold, preserved cadavers, ruling out osteoporosis with dual energy X-ray Absorptiometry (DEXA) scan studies. We removed all soft tissues, kept the ligaments and intervertebral discs, and sectioned the spines at the T<sub>12</sub>-L<sub>1</sub> disc and the sacroiliac joints. We performed CT scan studies (GE Healthcare, Milwaukee, WI, USA) with 0.625 mm section images. We examined these section images with a 1.25 mm collimation and a pitch of 3 (0.75 mm/rotation) from L<sub>1</sub> to the coccyx, reconstructing them in 3D with an *x-y* matrix of 512 × 512, an isotropic voxel of 1 × 1 × 1 mm, and a 0.5 mm slice spacing. We transferred the CT scan images to digital imaging and communications in medicine (DICOM). We measured each vertebra and intervertebral disc size and dimensions. We performed the MRI studies with a 1.5 Tesla GE MRI scan (GE Healthcare, Milwaukee, WI, USA), looking for disc degeneration and zygapophyseal joint osteoarthritis.

We analyzed CT and MRI scan images with the NETEOUS program, developed at the Biomechanics Institute of Valencia in collaboration with INGECOT (University of Oviedo, Asturias, Spain).

We obtained morphological data about geometry, morphometry, and dimensions of each lumbar and sacral vertebra and the intervertebral discs. In addition, we calculated anteroposterior (AP) and lateral (L) vertebral endplate dimensions, as well as the height and angulation of each intervertebral disc.

This lumbar spine model is a parametric model programmed in APDL ("Ansys Parametric Design Language"). The model can draw any section of the lumbar spine starting from sagittal plane radiography. We can change the different parameters in the model, the geometry of the vertebrae, the model mesh, and the material's mechanical properties. For each vertebra, the coordinates of four points are necessary to reproduce its geometry and position in the lumbar spine model. We calculated the rest of the parameters to build the model using formulas derived from the study by Panjabi et al. [33].

We can change the parameters of the mesh. We obtain the mesh by dividing the vertebra into different regions. One or more combined parameters control the mesh density of

other areas. The higher the mesh density, the higher the accuracy of calculations and the computation time.

In the model, the vertebra is composed of three different elements. First, the vertebral body consists of cancellous bone and an outer layer of cortical bone. We modelled the posterior arch with a specific material for that area.

The intervertebral discs are composed of three elements: fibrous annulus, nucleus, and annulus fibers. We oriented the fibers as in an intact disc.

We included all the ligaments of the lumbar spine in the model. The ligaments have a nonlinear behavior. With small deformations, the ligaments have a low elastic modulus, but with a specific strain, the elastic modulus increases. Each ligament is modelled with two parallel links of two different materials to simulate the nonlinear behavior.

Apart from the intervertebral disc, each vertebra articulates with the adjacent vertebra through the upper and lower zygapophyseal joints. These joints are responsible for the transmission of a large portion of loads between the vertebrae. We modelled the contacts in the zygapophyseal joints with particular contact elements. The material properties in zygapophyseal joint contacts are specific.

Once we had obtained its final 3D geometry with CAD software for the biomechanical evaluation of a new nucleus implant, we imported it into *Ansys* for finite element modelling. Then, we assigned mesh properties and materials' mechanical properties to the implant and used four-node solid elements for the mesh.

This simple geometry represents the first approach for the biomechanical evaluation of a nucleus implant.

We evaluated two design groups, monobloc and sandwich-type. First, we selected the materials for each design type. Then, we evaluated each design with FEA. Finally, we evaluated eighteen original designs to find the one that is the most suitable for the particular characteristics needed for a nucleus disc replacement.

**2.1. Monobloc Designs.** Traditionally, monobloc designs have a single interface-free elastomeric material (hydrogel, PU, silicone). Their advantages are wearing and mechanical properties like the intact disc, and their drawback is the extrusion risk. In addition, the compression required to insert these designs could lead to damage and accelerated degradation. Figure 1 shows the monobloc designs evaluated in this study.

**2.2. Sandwich Designs.** They consist of two different materials, one for the outer component, which encloses an inner one. The outer material is usually stiff PEEK (Polyetheretherketone), Polyethylene (PE). The inner is viscoelastic (PU, silicone, hydrogel) or a shape memory material (PU). The sandwich designs' advantages are their viscoelastic and tissue integration properties, which minimize migration and extrusion, and the disadvantage is their low compressibility, usually requiring a bigger annulotomy for its insertion.

Figure 2 shows the disc nucleus sandwich designs analyzed in this study. Figures 2(a)–2(c) show a rigid outer

shell (PEEK) and a hydrogel or viscoelastic shock-absorbing core. Figures 2(d)–2(f) show dampening designs, while Figures 2(g) and 2(h) show shape-memory models with two PEEK shells containing a shape-memory polymer (PU). Figure 2(i) shows a hard outer shell and a softer viscoelastic core. Finally, Figure 2(j) shows an external bag filled with viscoelastic materials.

**2.3. Material Selection.** We tried PU, shape-memory polymers, PEEK, hydrogels, fabrics and blends, or compounds (i.e., carbon fiber-reinforced PEEK).

**2.4. Monobloc Design Material Selection.** We considered silicones, polyurethanes, and polycarbonate urethanes (PCUs).

**2.5. Sandwich Design Material Selection.** We evaluated propylene, polyethylene terephthalate + dimethyl siloxane, polyamide 6,6 plus polyethylene terephthalate for the bag, hydrogel, ultrahigh molecular weight polyethylene (UHMWPE), PEEK, PU that cures at body temperature, and elastomeric microspheres for the core.

**2.6. Selection Criteria.** We were interested in a nucleus replacement that was easy to insert through a minimal annulectomy, mechanical behavior like the natural nucleus, and minimal wear and tear.

**2.7. Design Analysis.** We performed design analysis by simulation with FEA under physiological loading conditions, analyzing stresses, and deformations in compression and shear.

**2.7.1. Compression Test.** We applied a compressive force to a standard cylinder (a diameter of  $29 \text{ mm} \pm 0.5 \text{ mm}$  and a height of  $12.5 \text{ mm} \pm 0.5 \text{ mm}$ ), obtaining force/deformation curves. We performed four compression cycles, considering the fourth at 10% and 20% deformation. We evaluated the implant under different physiological load cases [10]: axial compression of 1000 N (compression load on the lumbar spine during walking), axial compression of 1000 N and anterior-posterior shear of 300 N (normal load combination typical of walking activity), axial compression of 1000 N, flexion moment of 8 Nm in the sagittal plane, and axial rotation torque of 8 Nm (representative of a worst-case scenario, with a high potential for producing disc herniation).

We considered fixing the displacements and rotations of nodes below the lower vertebra to apply loads. We joined the nodes in the upper vertebra's upper edge to the upper vertebra's superior central node with links elements. Then, we merged the nodes of the spinous process with the previous structure with link elements. Next, we spread the load evenly with this structure. Finally, we placed the loads in the top central node of the upper vertebra; this node is the central node of the structure described above.

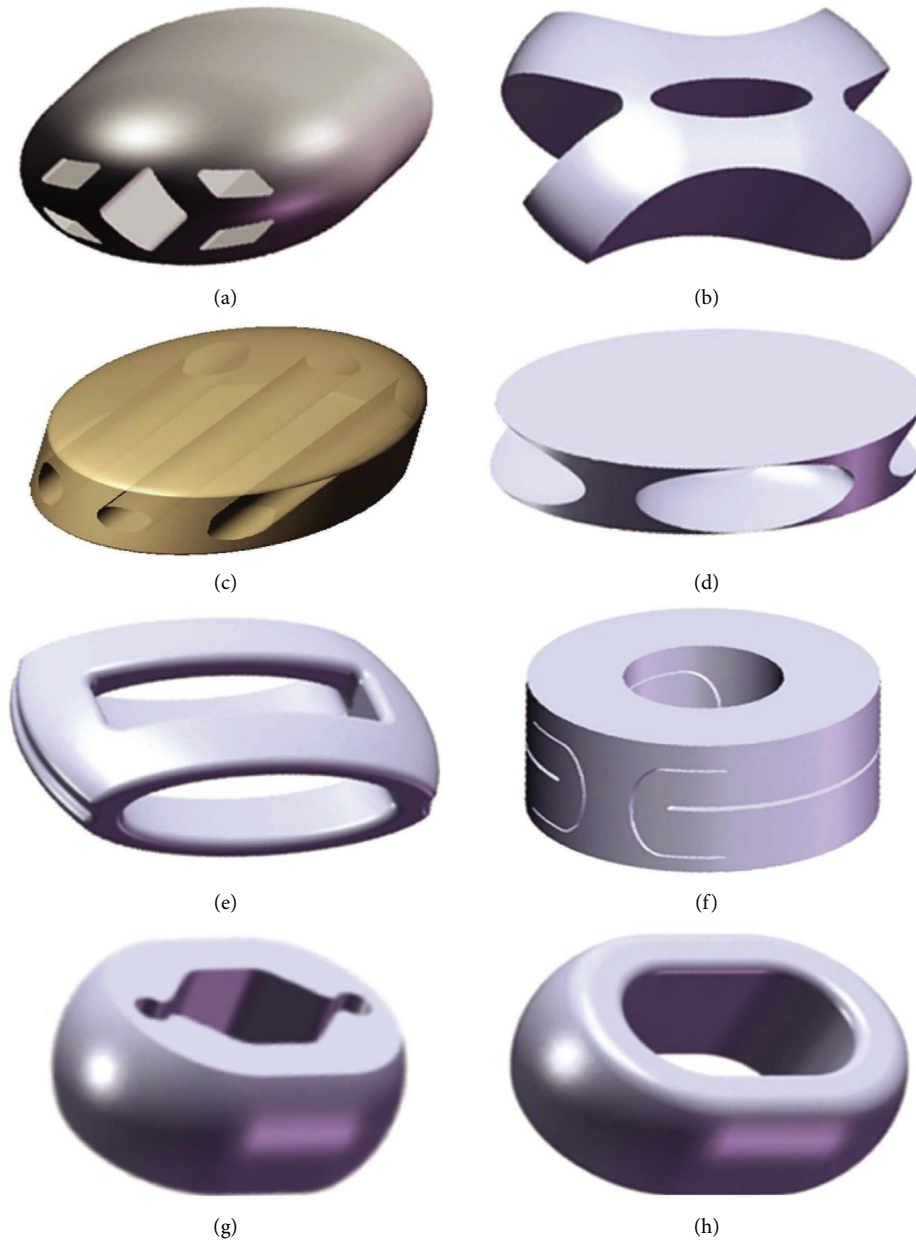


FIGURE 1: Monobloc designs evaluated in our study that aimed to optimize insertion and mechanical properties.

**Shear test.** We used four identical parallelepiped pieces,  $4 \text{ mm} \pm 1 \text{ mm}$  thick,  $20 \text{ mm} \pm 5 \text{ mm}$  wide, and  $25 \text{ mm} \pm 5 \text{ mm}$  long, bonded with a high modulus adhesive on their two largest opposite faces to 4 rigid plates of the same width and length on a sandwich arrangement. We obtained a force/deformation curve, calculating the shear modulus at a 25% shear stress using the formula  $\gamma = d/2c$ , where  $d$  is the test piece deformation and  $c$  is the tested element thickness, both in millimeters. First, we calculated the 25% shear stress using  $\tau_{25} = F_{25}/2A$  ( $F$  force in Newtons and  $A$  test pieces' bonded area in  $\text{mm}^2$ ). Next, we calculated the shear modulus  $G$  ( $\text{N}\cdot\text{mm}^{-2}$ ) using  $G = \tau_{25}/\gamma_{25} = \tau_{25}/0.25$ . Finally, we repeated the test three times, obtaining a mean value.

**2.8. Anatomical Data.** We obtained these data from plain lumbar spine sagittal radiography and 1.5 Tesla Magnetic Resonance Images of human spine specimens and processed them with Materialise's software Mimics v.11, building three-dimensional images. We calculated the intervertebral nucleus's volume and shape (length, size, and width) and transformed them into a CAD (computer-aided design) file. We validated the implant biomechanical geometry with finite element analysis (FEA) using the image analysis data and the lumbar spine model programmed in APDL ("Ansys Parametric Design Language") (Figure 3). We used the data from our previous studies [32]. In addition, we obtained data from the literature [34] the spinal elements' mechanical properties.

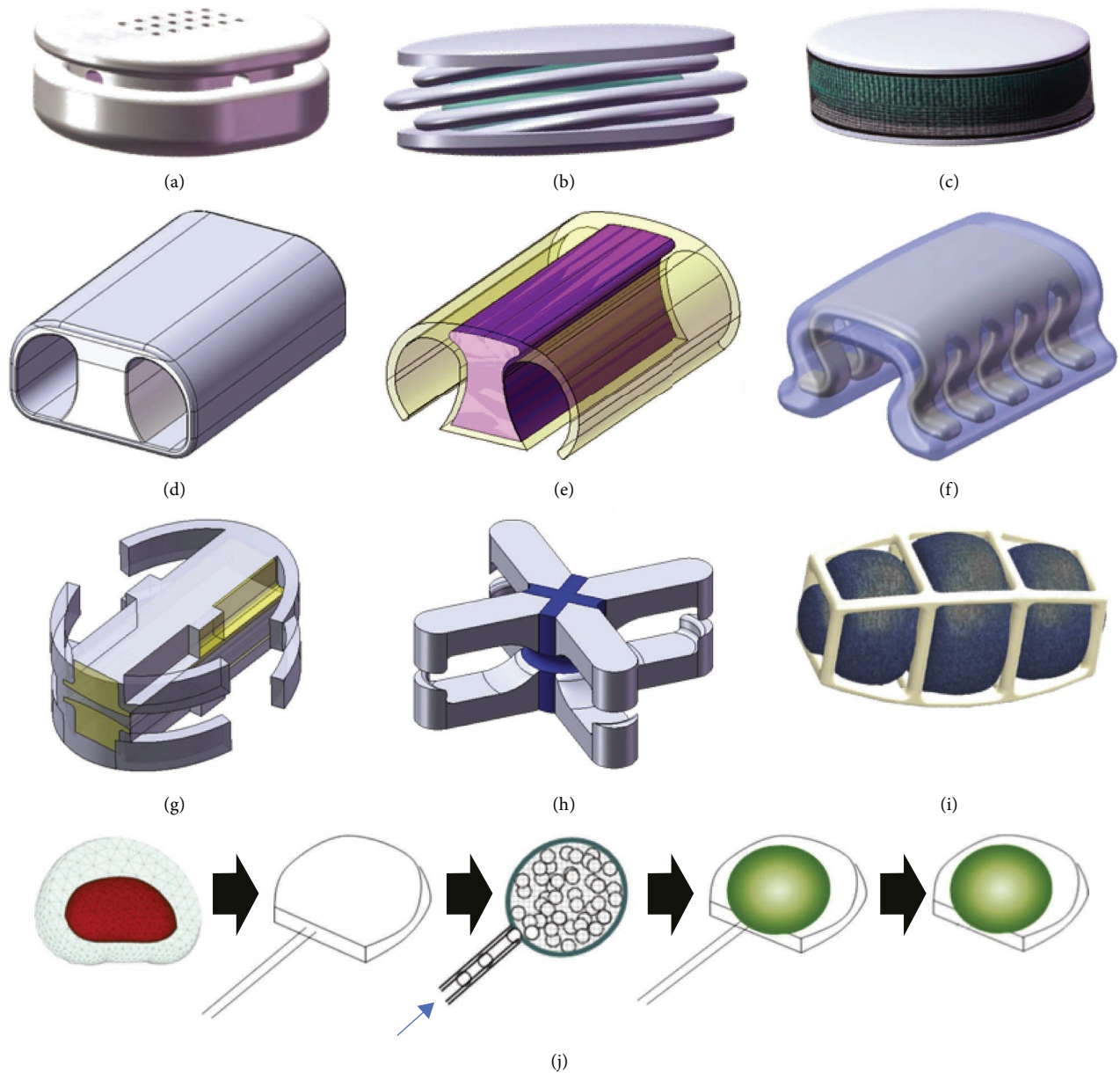


FIGURE 2: Sandwich designs that we evaluated in this study. We can group them into shock absorbing (a–c), dampening (d–f), shape memory (g–i), and balloon type (j).

**2.9. Nucleus Replacement FEA Evaluation.** To study which design suited our requirements, we performed FEA compression (BS ISO 7743:2008) and shear modulus tests (BS ISO 1827:2007). We applied 1000 N axial compression (like lumbar spine load during walking), 1000 N axial compression plus 300 N anteroposterior shear, and 1000 N axial compression with an 8 Nm sagittal plane flexion moment plus axial 8 Nm rotation torque (the scenario with a high risk of disc herniation).

We spread the load evenly within this structure and placed it in the upper vertebra's top central node. We performed all simulations with the implant located at the lumbar segment L<sub>4</sub>–L<sub>5</sub>. After implant insertion, we did not close the 8 mm annulus defect necessary to insert the implants.

### 3. Results

The selected monobloc elastomeric design bore physiological stresses correctly in FEA studies (Figure 4(a)) but suffered significant deformations during insertion (Figure 4(c)). Therefore, we used reinforced polyurethane (a composite) or polyurethane carbonate (PCU) and ruled out PEEK and rigid polymers.

FEA studies of sandwich designs showed that those with a hard inner core (PEEK) and a softer outer component were too stiff (Figure 5(b)). Although they had acceptable lateral compressibility for the introduction (Figure 5(a)), their insertion required an annulotomy of at least 18 mm in length. Others had excessive wear. Furthermore, sandwich



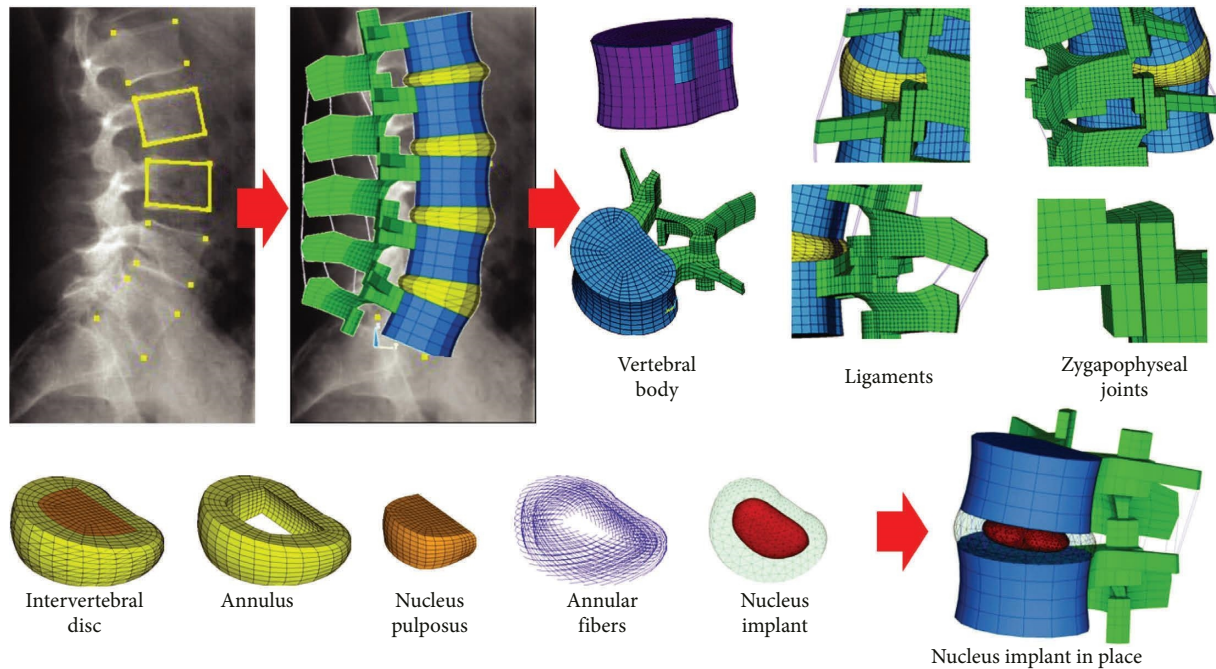


FIGURE 3: FEA model that we used in this study.

designs with a stiff core and small endplate contact area had a high subsidence risk (Figures 4(c) and 4(d)).

After the study, we chose an oval doughnut-like hollow compressible monobloc elastomeric design with a 5 mm wall (Figures 5(a) and 5(b)). In FEA analysis, it minimized implant stress under loading conditions, distributed strains uniformly, and tolerated the lateral compression during implantation.

#### 4. Material Selection

We searched extensively to select the material that best simulated the biomechanical behavior of the nucleus pulposus. Silicones were ruled out because they crack and fracture over time [25], and polyurethanes were too rigid [35], but polycarbonate polyurethanes [36] suited our requirements. Therefore, we chose Bionate® (Polymer Technology Group DSM-PTG, Berkeley, California, USA) [37]. It is available in 55D, 65D, 75D, 80A, and 90A ([https://www.dsm.com/content/dam/dsm/biomedical/en\\_us/documents/document-bionate-pcu-productsheet.pdf](https://www.dsm.com/content/dam/dsm/biomedical/en_us/documents/document-bionate-pcu-productsheet.pdf)). Considering their published mechanical properties [38], we selected 55D, 80A, and 90A for further analysis.

**4.1. Nucleus Replacement Biomechanical Results.** Comparing the three types of Bionate® selected for our design, 80A has the lowest Z-axis displacement and stresses under the 1000 N axial load, even when combined with 300 N anteroposterior shear and 8 Nm rotation torque, favoring fatigue endurance. Implant stresses increase with material hardness for all axes and are higher for 90A than 80A, with no significant difference between 90A and 55D

(Table 1 and Figure 6). The maximum stresses happen on the Z-axis.

**4.2. Annulus Stresses.** Under 1000 N axial compression, all three Bionate® types induced similar annulus stresses, being maximum on the Z-axis. Adding 300 N anteroposterior shear Bionate® 80A made the annulus bear more load than 90A and 55D. The maximum stress also happened on the Z-axis. When adding 8 Nm rotation torque, the annulus supported the highest stresses with Bionate 80A. Again, 80A shared more load with the annulus than 90A and 55D, which had a similar behavior (Table 2 and Figure 7). Higher annulus stress for the Bionate® 80A nucleus replacement indicates that it distributes the load to the ring apophysis not to the vertebral endplates, making the subsidence risk smaller.

Bionate® 80A produced stresses remarkably close to those achieved with the natural disc nucleus, an extraordinarily positive feature since avoiding annulus relaxation is crucial for the nucleus implant.

**4.3. Vertebral Endplate Contact Pressures.** The greater the material's rigidity, the greater the contact stresses transmitted to the bone; therefore, the subsidence risk increases when faced with very high loads. For example, under 1000 N axial compression loads, even when adding 300 N anteroposterior shear and 8 Nm rotational torque, the lowest is for Bionate® 80A (Table 3 and Figure 8). This type of Bionate® exerts more evenly load distribution than 90A and 55D and thus has a smaller chance of subsidence, corroborating the data from annulus stresses. Therefore, after all the FEA, the data show that Bionate® 80A is the most suitable material for nucleus replacement since its biomechanical behavior is like the

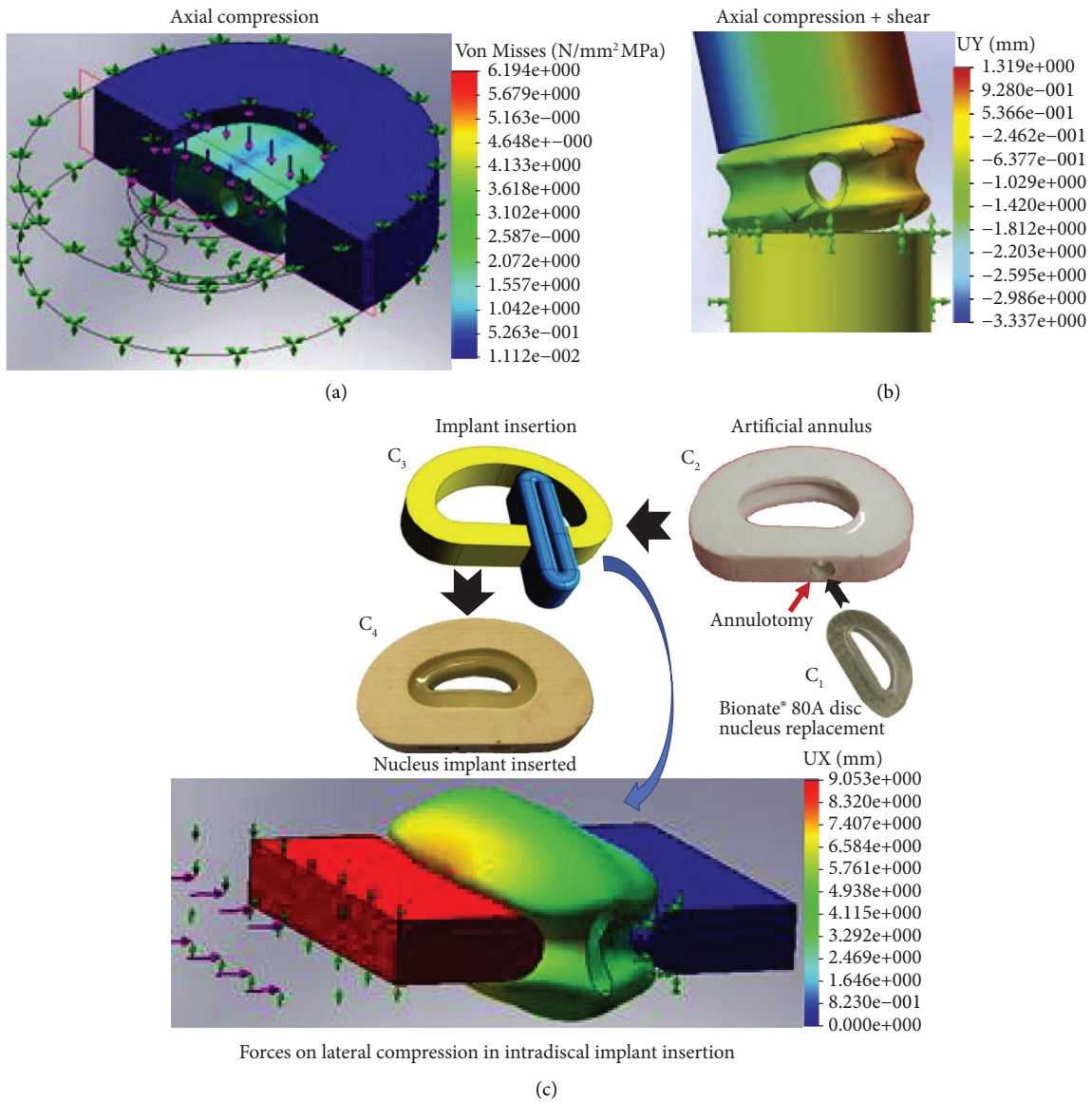


FIGURE 4: Selected monobloc elastomeric device FEA studies during (a) axial compression, (b) lateral compression, and (c) axial compression plus shear. Implant deformations in the x (UX) and y (UY) axes.

natural one. We found that the implant manufactured with Bionate® 80A has a stiffness of 862.81 N/mm.

**5. Discussion**

After carrying out all the designs and tests of different materials, the PCU material imitates intact nucleus characteristics, particularly Bionate®. Although manufacturers can provide it with different hardness, Bionate® 80A is best suited for nucleus replacements as its properties are the closest to the intact nucleus [38]. On the other hand, more rigid types (55D, 75D, 90A) deform more and distribute loads more unevenly, inducing a higher subsidence risk [37].

The nucleus replacements need an intact annulus fibrosus to contain the implant in its place. Therefore, this

always requires an annulotomy. However, the minimally invasive approach severely limits implant materials and designs. Bionate® 80A is elastic enough to tolerate compression during insertion, [38] facilitating a smaller annulotomy. An alternative is to perform an annulus repair [30].

Additionally, Bionate® 80A has a 35/65 (weight/weight) hard-to-soft segment ratio [39], fluid-film lubrication [40], and wear and friction characteristics superior to metal UHMWPE [41]. It has high resistance to abrasion, tear, hydrolysis, and ageing [42].

The different Bionate's® coefficient friction is 0.64 for 75D, 0.81 for 55D, and 1.52 for 80A. This value over one means that Bionate® 80A has higher resistance than the normal force. Over ten loading cycles, Bionate® 80A Young's modulus increased from 22.19 MPa to 23.93 MPa

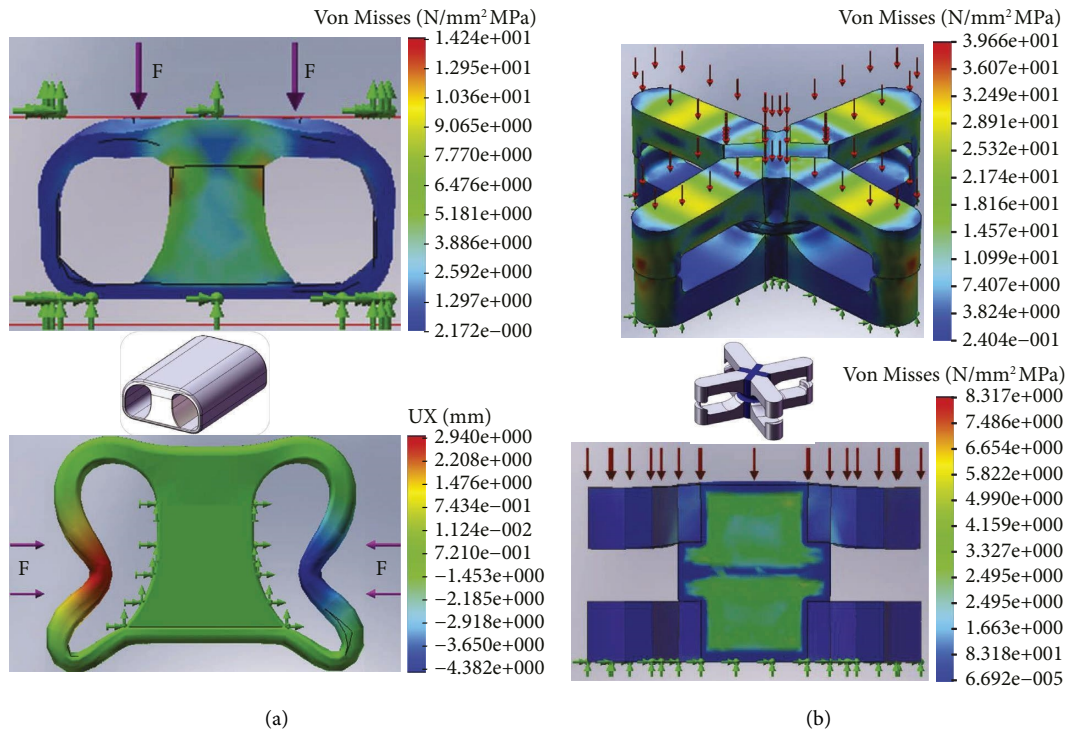


FIGURE 5: Finite element analysis of two sandwich-type nucleus implants. Implant deformations in the  $x$ -axis (UX).

and Poisson's ratio was 0.49 (39). Bionate 75D Young's modulus increased from 131.1 MPa to 327.6 MPa, and Poisson's ratio decreased from 0.43 to 0.38 [38]. These data confirm that Bionate® 80A has the best mechanical properties for a nucleus replacement.

PCU particles cause a lesser inflammatory reaction in implant wear than metal or UHMWPE [43]. In addition, our group saw that Bionate 80A particles induce no local or distant tissue adverse reactions [44]. Therefore, we recommend using best long-term endurance PCU, Bionate® 80A.

The design is crucial as the shape and size of the nucleus replacement decisively influence the annulotomy size. An injectable material curing *in situ* after the discectomy would be ideal, but achieving it regularly and reliably is challenging. The reagent mix, temperature, and curing time require strict control for steady results. Additionally, polymerizing agents are cytotoxic, so excess or leaching might have negative consequences. An option is to use a bag subsequently filled with elastomeric self-curing liquid. These bags, usually made of porous materials to ease nearby bone and annulus fixation, allow toxic reagent mix diffusion. A smooth non-permeable bag would not adhere to nearby tissues, facilitating extrusion, a critical complication of nucleus replacement devices. As a result, the devices that have reached clinical application [45] have limited use.

Monobloc designs are simpler to manufacture with regular results and more straightforward to customize. However, these nucleus replacements often require a larger annulotomy, increasing the extrusion risk unless we can deform and compress them when inserted. That is why Bionate® 80A is particularly suited for nucleus replacements, and our design fulfils this requirement. We found that the implant manufactured with Bionate® 80A has a stiffness (Table 1) of 862.81 N/mm, and stiffness is between the value of 667 N/mm on average for the L<sub>1</sub>–L<sub>5</sub> discs and 1000 N/mm for the whole L<sub>5</sub>–S<sub>1</sub> segment, which is in the range of the studies carried out by White and Panjabi (1990) (12).

A final consideration is that the strongest endplate area is the so-called ring apophysis, a solid cortical bone hoop at its periphery [46]. Therefore, any implant transmitting the load mainly to this apophysis has the lowest subsidence risk. The rationale behind our nucleus replacement design is to maximize the load transmission to the ring apophysis and minimize it to the rest of the vertebral endplate.

The most significant limitation of our study is that we took from the literature the properties needed to reproduce those of an intact disc nucleus which we should customize for any specific patient needing this procedure. Furthermore, the evaluation of joint implants with FEA or FEM,



BIONATE® NUCLEUS REPLACEMENT

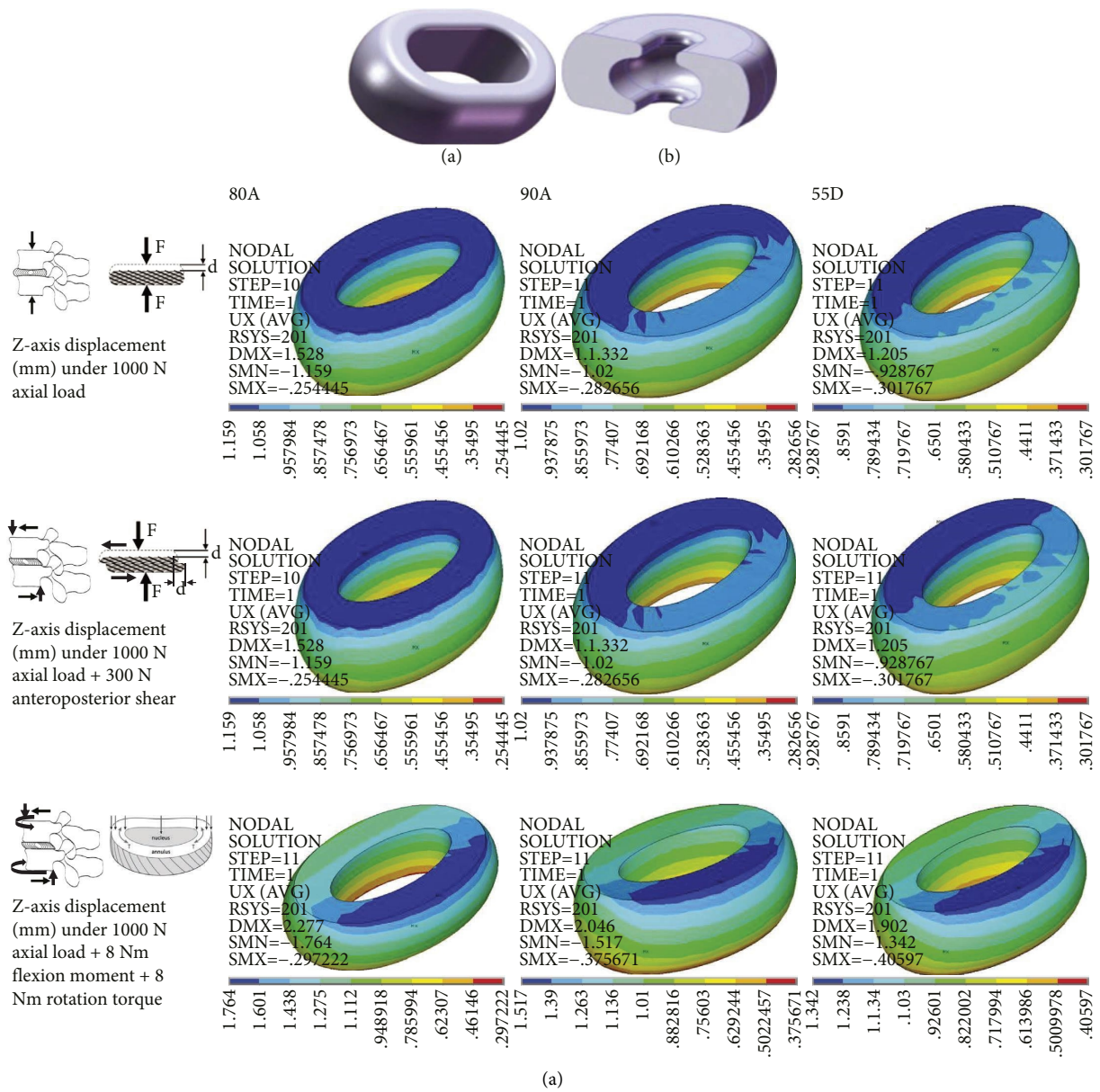


FIGURE 6: Continued.

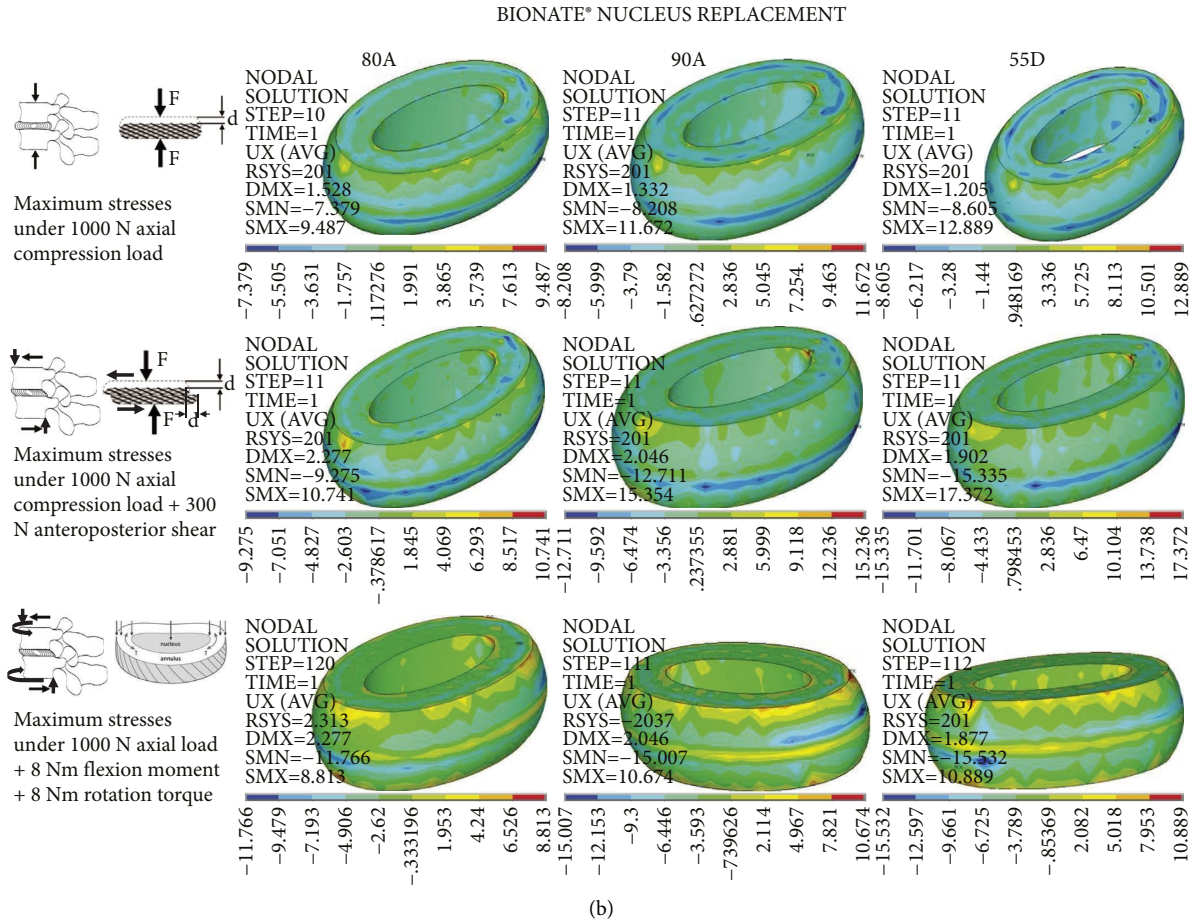


FIGURE 6: (a) Monobloc design selected and (b) coronal section. Nucleus replacement biomechanical characteristics comparing the three Bionate® chosen types.

TABLE 1: Bionate® nucleus replacement properties comparing the three types of this material. We shaded the maximum results in blue.

Nucleus replacement data with Bionate®	80 A	90 A	55D	
Z-axis displacement (mm) under 1000 N axial compression load	1.159	1.02	0.93	
Z-axis displacement (mm) under 1000 N axial load + 300 N anteroposterior shear	1.76	1.517	1.342	
Z-axis displacement (mm) under 1000 N axial load + 8 Nm flexion moment + 8 Nm rotation torque	1.839	1.554	1.361	
Maximum stresses under 1000 N axial compression load	Sx (MPa)	5.1	5.42	5.38
	Sy (MPa)	5.35	5.79	5.84
	Sz (MPa)	5.5	6	6.22
Maximum stresses under 1000 N axial compression load + 300 N anteroposterior shear	Sx (MPa)	6.33	8.5	10.4
	Sy (MPa)	6.55	8.9	10.9
	Sz (MPa)	7.05	9.6	11.7
Maximum stresses under 1000 N axial load + 8 Nm flexion moment + 8 Nm rotation torque	Sx (MPa)	6.7	11.6	11.3
	Sy (MPa)	6.6	11.3	11.5
	Sz (MPa)	7.2	12.1	12.6

TABLE 2: Maximum annulus stresses with the selected design nucleus replacement made of Bionate® 80 A, 90 A, and 55D.

Annulus stress with nucleus replacement with Bionate®	80 A	90 A	55D	
Maximum stresses under 1000 N axial compression load	Sx (MPa)	1.27	1.25	1.24
	Sy (MPa)	1.21	1.2	1.17
	Sz (MPa)	1.64	1.63	1.61
Maximum stresses under 1000 N axial compression load + 300 N anteroposterior shear	Sx (MPa)	1.5	1.2	1.12
	Sy (MPa)	1.48	1.12	1
	Sz (MPa)	2.16	1.7	1.6
Maximum stresses under 1000 N axial load + 8 Nm flexion moment + 8 Nm rotation torque	Sx (MPa)	1.66	1.3	1.14
	Sy (MPa)	1.63	1.2	1.1
	Sz (MPa)	2.1	1.8	1.71

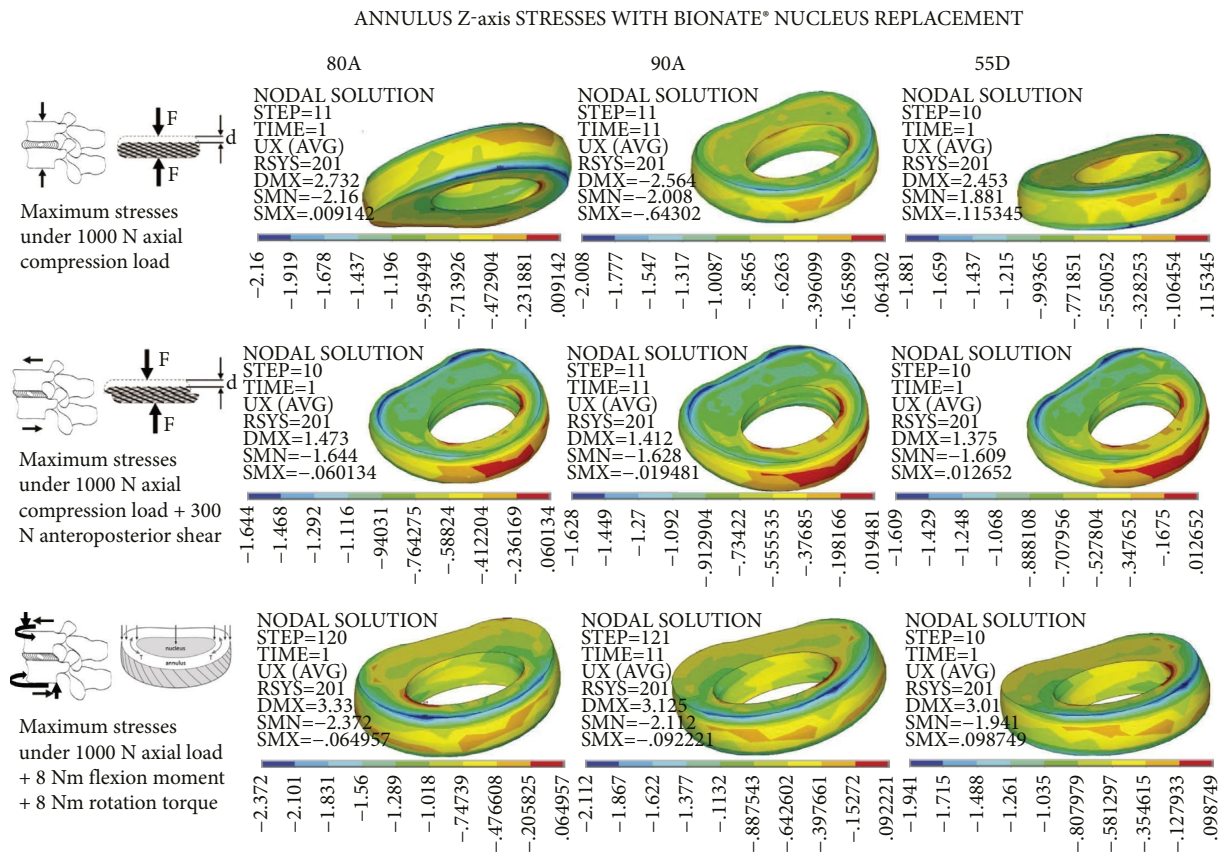


FIGURE 7: Annulus Z-axis stresses with the selected design Bionate® nucleus replacement 80 A, 90 A, and 55D.

TABLE 3: The vertebral endplates' maximum contact pressures with the selected design nucleus replacement made of Bionate® 80 A, 90 A, and 55D.

Vertebral endplate contact pressures with nucleus replacement with Bionate®	80 A	90 A	55D
Maximum contact pressures 1000 N axial compression load	0.719	0.98	1.09
Maximum contact pressures 1000 N axial compression load + 300 N anteroposterior shear	1.159	1.614	1.935
Maximum contact pressures 1000 N axial compression load + 8 Nm flexion moment + 8 Nm rotation torque	1.262	1.701	2.033



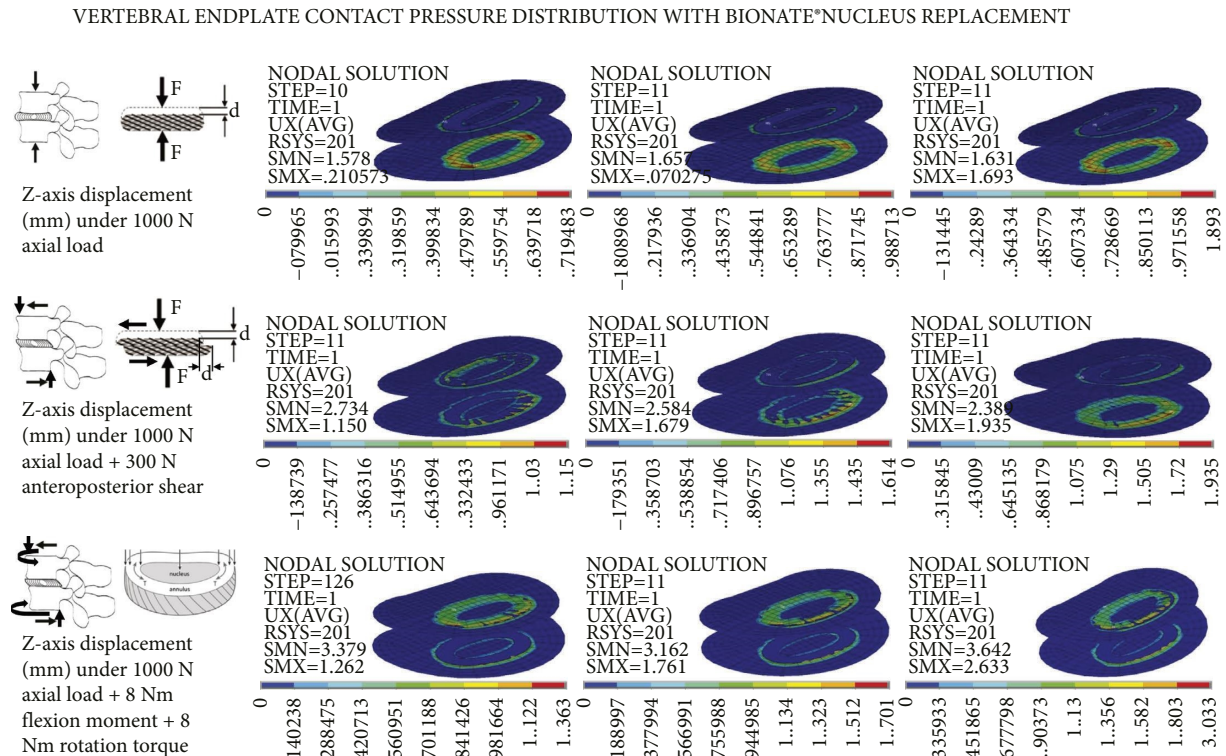


FIGURE 8: Contact pressure distribution on the vertebral endplates with the selected design nucleus replacement made of Bionate® 80 A, 90 A, or 55D under 1000 N axial compression load.

besides being patient-specific, is also very time consuming. Meshing bones and soft tissues is complicated. In addition, we need to study if the material suffers deterioration and cracking under long-term use.

We have performed an FEA of several designs and materials and found the best to replace the nucleus pulposus. In addition, we have developed a lumbar spine model with the patient's radiological images (plain X-ray and MRI). This model allows nucleus replacement customization.

## 6. Conclusions

Of all materials we analyzed, Bionate® 80A has mechanical characteristics closest to the natural nucleus and is the most suitable for the nucleus replacement.

Bionate® 80A yields the lowest implant stress due to compressive forces (favoring fatigue endurance), produces the highest stress level in the annulus (closest to the natural nucleus), and has the lowest subsidence risk. Unfortunately, all these features worsen directly proportional to material hardness.

Out of the eighteen designs we analyzed with FEA, we found that the monobloc oval doughnut-like Bionate 80A nucleus replacement reproduced the best biomechanics of the natural disc nucleus and had the lowest subsidence risk as it transmits the load to the ring apophysis. Furthermore, implanting it through the annulotomy required to perform a lumbar microdiscectomy should be possible due to its elasticity.

## Data Availability

Data are available on request from the corresponding author.

## Conflicts of Interest

The authors declare no conflicts of interest.

## Acknowledgments

"This work was supported by the European Union's 6th Framework Programme under project number IP 026599-s".

## References

- [1] J. W. S. Vlaeyen, C. G. Maher, K. Wiech et al., "Low back pain," *Nature Reviews Disease Primers*, vol. 4, no. 1, p. 52, 2018.
- [2] M. J. DePalma, J. M. Ketchum, T. R. Saullo, and B. L. Laplante, "Is the history of a surgical discectomy related to the source of chronic low back pain?" *Pain Physician*, vol. 15, no. 1;1, pp. E53–E58, 2012.
- [3] M. L. Vraa, C. A. Myers, J. L. Young, and D. I. Rhon, "More than 1 in 3 patients with chronic low back pain continue to use opioids long-term after spinal fusion: a systematic review," *The Clinical Journal of Pain*, vol. 38, no. 3, pp. 222–230, 2022.
- [4] G. Tendulkar, T. Chen, S. Ehnert, H. P. Kaps, and A. K. Nüssler, "Intervertebral disc nucleus repair: hype or hope?" *International Journal of Molecular Sciences*, vol. 20, no. 15, p. 3622, 2019.



- [5] S. A. Rundell, H. L. Guerin, J. D. Auerbach, and S. M. Kurtz, "Effect of nucleus replacement device properties on lumbar spine mechanics," *Spine*, vol. 34, no. 19, pp. 2022–2032, 2009.
- [6] A. N. Sieber and J. P. Kostuik, "Concepts in nuclear replacement," *The Spine Journal*, vol. 4, no. 6, pp. 322S–324S, 2004.
- [7] Y. C. Huang, Y. Hu, Z. Li, and K. D. K. Luk, "Biomaterials for intervertebral disc regeneration: current status and looming challenges," *J Tissue Eng Regen Med*, vol. 12, no. 11, pp. 2188–2202, 2018.
- [8] V. Ellä, M. Kellomäki, and P. Törmälä, "In vitro properties of PLLA screws and novel bioabsorbable implant with elastic nucleus to replace intervertebral disc," *Journal of Materials Science: Materials in Medicine*, vol. 16, no. 7, pp. 655–662, 2005.
- [9] W. J. Virgin, "Experimental investigations into the physical properties of the intervertebral disc," *Journal of Bone and Joint Surgery British Volume*, vol. 33-B, no. 4, pp. 607–611, 1951.
- [10] H. J. Wilke, P. Neef, M. Caimi, T. Hoogland, and L. E. Claes, "New in vivo measurements of pressures in the intervertebral disc in daily life," *Spine*, vol. 24, no. 8, pp. 755–762, 1999.
- [11] T. Brown, R. J. Hansen, and A. J. Yorra, "Some mechanical tests on the lumbosacral spine with particular reference to the intervertebral discs; a preliminary report," *The Journal of Bone and Joint Surgery*, vol. 39, no. 5, pp. 1135–1164, 1957.
- [12] A. A. White and M. M. Panjabi, *Clinical Biomechanics of the Spine*, 722, 2nd edition, Lippincott, Philadelphia, PA, USA, 1990.
- [13] J. C. Iatridis, L. A. Setton, M. Weidenbaum, and V. C. Mow, "The viscoelastic behavior of the non-degenerate human lumbar nucleus pulposus in shear," *Journal of Biomechanics*, vol. 30, no. 10, pp. 1005–1013, 1997.
- [14] H. F. Farfan, J. W. Cossette, G. H. Robertson, R. V. Wells, and H. Kraus, "The effects of torsion on the lumbar intervertebral joints: the role of torsion in the production of disc degeneration," *The Journal of Bone and Joint Surgery*, vol. 52, no. 3, pp. 468–497, 1970.
- [15] B. Yu, C. Zhang, C. Qin, and H. Yuan, "FE modeling and analysis of L4-L5 lumbar segment under physiological loadings," *Technology and Health Care*, vol. 23, no. s2, pp. S383–S396, 2015.
- [16] J. M. Cloyd, N. R. Malhotra, L. Weng, W. Chen, R. L. Mauck, and D. M. Elliott, "Material properties in unconfined compression of human nucleus pulposus, injectable hyaluronic acid-based hydrogels and tissue engineering scaffolds," *European Spine Journal*, vol. 16, no. 11, pp. 1892–1898, 2007.
- [17] J. C. Iatridis, L. A. Setton, M. Weidenbaum, and V. C. Mow, "Alterations in the mechanical behavior of the human lumbar nucleus pulposus with degeneration and aging," *Journal of Orthopaedic Research*, vol. 15, no. 2, pp. 318–322, 1997.
- [18] R. R. Patel, A. Noshchenko, R. Dana Carpenter et al., "Evaluation and prediction of human lumbar vertebrae endplate mechanical properties using indentation and computed tomography," *Journal of Biomechanical Engineering*, vol. 140, no. 10, 2018.
- [19] H. Schmidt, F. Galbusera, A. Rohlmann, and A. Shirazi-Adl, "What have we learned from finite element model studies of lumbar intervertebral discs in the past four decades?" *Journal of Biomechanics*, vol. 46, no. 14, pp. 2342–2355, 2013.
- [20] Z. C. Zhong, S. H. Wei, J. P. Wang, C. K. Feng, C. S. Chen, and C. h Yu, "Finite element analysis of the lumbar spine with a new cage using a topology optimization method," *Medical Engineering & Physics*, vol. 28, no. 1, pp. 90–98, 2006.
- [21] P. Borkowski, P. Marek, G. Krzesiński et al., "Finite element analysis of artificial disc with an elastomeric core in the lumbar spine," *Acta of Bioengineering and Biomechanics*, vol. 14, no. 1, pp. 59–66, 2012.
- [22] J. H. Lee, W. M. Park, Y. H. Kim, and T. A. Jahng, "A biomechanical analysis of an artificial disc with a shock-absorbing core property by using whole-cervical spine finite element analysis," *Spine*, vol. 41, no. 15, pp. E893–E901, 2016.
- [23] E. Wagnac, P. J. Arnoux, A. Garo, and C. E. Aubin, "Finite element analysis of the influence of loading rate on a model of the full lumbar spine under dynamic loading conditions," *Medical, & Biological Engineering & Computing*, vol. 50, no. 9, pp. 903–915, 2012.
- [24] D. G. T. Strange, S. T. Fisher, P. C. Boughton, T. J. Kishen, and A. D. Diwan, "Restoration of compressive loading properties of lumbar discs with a nucleus implant—a finite element analysis study," *The Spine Journal*, vol. 10, no. 7, pp. 602–609, 2010.
- [25] L. Grassner, A. Grillhösl, M. Bierschneider, and M. Strowitzki, "Disc herniation caused by a viscoelastic nucleus after total lumbar disc replacement—a case report," *Journal of Spine Surgery*, vol. 4, no. 2, pp. 478–482, 2018.
- [26] N. R. Ordway, W. F. Lavelle, T. Brown, and Q. B. Bao, "Biomechanical assessment and fatigue characteristics of an articulating nucleus implant," *The International Journal of Spine Surgery*, vol. 7, no. 1, pp. e109–e117, 2013.
- [27] Z. m. Zhang, L. Zhao, D. b. Qu, and D. d. Jin, "Artificial nucleus replacement: surgical and clinical experience," *Orthopaedic Surgery*, vol. 1, no. 1, pp. 52–57, 2009.
- [28] C. Li, J. Chen, Y. Lv et al., "Recent progress in electrospun nanofiber-based degenerated intervertebral disc repair," *ACS Biomaterials Science & Engineering*, vol. 8, no. 1, pp. 16–31, 2022.
- [29] S. L. Marshall, T. D. Jacobsen, E. Emsbo et al., "Three-dimensional-printed flexible scaffolds have tunable biomimetic mechanical properties for intervertebral disc tissue engineering," *ACS Biomaterials Science & Engineering*, vol. 7, no. 12, pp. 5836–5849, 2021.
- [30] S. Kirnaz, S. Singh, C. Capadona et al., "Innovative biological treatment methods for degenerative disc disease," *World Neurosurgery*, vol. 157, pp. 282–299, 2022.
- [31] A. Matta, M. Z. Karim, H. Gerami, B. Benigno, and W. M. Erwin, "A comparative study of mesenchymal stem cell transplantation and NTG-101 molecular therapy to treat degenerative disc disease," *Scientific Reports*, vol. 11, no. 1, Article ID 14804, 2021.
- [32] A. Vanaclocha-Saiz, C. M. Atienza, V. Vanaclocha et al., "ICR in human cadaveric SPECIMENS: an essential parameter to consider in a new lumbar disc prosthesis DESIGN," *North American Spine Society Journal (NASSJ)*, vol. 2, Article ID 100016, 2020.
- [33] M. M. Panjabi, V. Goel, T. Oxland et al., "Human lumbar vertebrae. Quantitative three-dimensional anatomy," *Spine*, vol. 17, no. 3, pp. 299–306, 1992.
- [34] L. X. Guo and W. Fan, "Impact of material properties of intervertebral disc on dynamic response of the human lumbar spine to vertical vibration: a finite element sensitivity study," *Medical, & Biological Engineering & Computing*, vol. 57, no. 1, pp. 221–229, 2019.
- [35] K. Uram, M. Kurańska, J. Andrzejewski, and A. Prociak, "Rigid polyurethane foams modified with biochar," *Materials*, vol. 14, no. 19, p. 5616, 2021.
- [36] J. A. M. Daniel Glad Stephen and M. Prakash, "The influence of the viscoelastic property of polycarbonate urethane as an

- artificial disc core material under various physiological motions at the L4-L5 level,” *The International Journal of Artificial Organs*, Article ID 3913988221116137, 2022.
- [37] C. Geary, C. Birkinshaw, and E. Jones, “Characterisation of Bionate polycarbonate polyurethanes for orthopaedic applications,” *Journal of Materials Science: Materials in Medicine*, vol. 19, no. 11, pp. 3355–3363, 2008.
- [38] N. Nic An Ghaill and E. G. Little, “Determination of the mechanical properties of Bionate 80A and Bionate 75D for the stress analysis of cushion form bearings,” *Proc Inst Mech Eng [H]*, vol. 222, no. 5, pp. 683–694, 2008.
- [39] M. J. Wiggins, M. MacEwan, J. M. Anderson, and A. Hiltner, “Effect of soft-segment chemistry on polyurethane biostability during in vitro fatigue loading,” *Journal of Biomedical Materials Research*, vol. 68A, no. 4, pp. 668–683, 2004.
- [40] C. Geary, E. Jones, D. Fitzpatrick, C. P. Kelly, and C. Birkinshaw, “In-vitro evaluation of a polyurethane compliant-layer glenoid for use in shoulder arthroplasty,” *Proceedings of the Institution of Mechanical Engineers*, vol. 224, no. 4, pp. 551–563, 2010.
- [41] S. C. Scholes, A. Unsworth, J. M. Blamey, I. C. Burges, E. Jones, and N. Smith, “Design aspects of compliant, soft layer bearings for an experimental hip prosthesis,” *Proceedings of the Institution of Mechanical Engineers*, vol. 219, no. 2, pp. 79–87, 2005.
- [42] M. C. Tanzi, S. Farè, and P. Petrini, “In vitro stability of polyether and polycarbonate urethanes,” *Journal of Biomaterials Applications*, vol. 14, no. 4, pp. 325–348, 2000.
- [43] R. A. Smith, A. Maghsoodpour, and N. J. Hallab, “In vivo response to cross-linked polyethylene and polycarbonate-urethane particles,” *Journal of Biomedical Materials Research Part A*, vol. 93, no. 1, pp. 227–234, 2010.
- [44] A. Vanaclocha-Saiz, V. Vanaclocha, C. Atienza et al., “Bionate biocompatibility: in vivo study in rabbits,” *ACS Omega*, vol. 7, no. 34, pp. 29647–29654, 2022.
- [45] J. D. Golan, F. Martens, J. Griebel, D. C. LoPresti, M. G. Hess, and M. Ahrens, “Long-term outcomes following lumbar nucleus replacement,” *The Internet Journal of Spine Surgery*, vol. 15, no. 6, pp. 1096–1102, 2021.
- [46] D. C. Briski, V. K. Goel, B. S. Waddell et al., “Does spanning a lateral lumbar interbody cage across the vertebral ring apophysis increase loads required for failure and mitigate endplate violation,” *Spine*, vol. 42, no. 20, pp. E1158–E1164, 2017.